Jordan Journal of Civil Engineering, Volume **14**, No. **3**, **2020**

Buckling Analysis Behavior of Functionally Graded Beams

Hassina Ziou [1)] *, Hamza Guenfoud [2)] and Mohamed Guenfoud [3)]

[1)] Senior Researcher, National Centre for Studies and Integrated Research on Building (CNERIB), Souidania, Algiers, Algeria.
* Corresponding Author. E-Mail: hassina.geniecivil@gmail.com
[2)] Doctor, Department of Civil Engineering, University of Guelma, Algeria.
E-Mail: hamzaguenfoud@gmail.com
[3)] Professor, Department of Civil Engineering, University of Guelma, Algeria.
E-Mail: gue2905m@yahoo.fr.

ABSTRACT

In this paper, the static-buckling behavior of functionally graded material (FGM) beams has been reported *via* the finite-element method. Two separate finite element formulations are developed, one based on Euler–Bernoulli theory and the other one on the Timoshenko beam theory. FGM beams have a smooth variation of material properties due to continuous (unbroken) change in micro-structural details. The variation of material properties is along the beam thickness and is assumed to trail a power-law of the volume fraction of the constituents, usually ceramic and metal. Principle of virtual work is used to obtain the finite element system of equations. The stiffness and the geometrical stiffness matrix of FGM beams are given in detail as they have not been presented before. The model has been evaluated and validated with benchmark results available in the literature and a good agreement was found. Finite element numerical results are presented in tabulated and graphical forms to figure out the effects of power-law index, slenderness ratio and boundary conditions on buckling analysis of FGM beams.

KEYWORDS: Buckling analysis behavior, Finite element method, Euler-Bernoulli beam theory, Timoshenko beam theory.

INTRODUCTION

Functionally graded materials (FGMs) are advanced composite materials that have a gradual variation of the volume fractions of their constituents. This variation in composition leads to a continuity of the material properties from one surface to another and thus eliminates the stress concentration along the interfaces of the layers found in conventional laminated composite structures. FGMs are usually made of a mixture of ceramic and metal. The ceramic constituent of the material can withstand high temperatures in thermal environments due to its high temperature resistance, whereas the metal constituent obstructs the fracture caused by thermal stress due to its toughness and malleability. FGMs found their applications in various fields, such as aerospace and aeronautics, power plants, nuclear and civil engineering, among others.

Received on 30/1/2020.
Accepted for Publication on 22/5/2020.

A brief review of papers closely related to the current study is presented as follows: Akbaş (2015) studied post-buckling analysis of an axially functionally graded (AFG) cantilever beam subjected to an axial non-follower compression load. Rezaiee-Pajand and Masoodi (2016) developed exact free vibration and buckling solution of functionally graded material tapered beam-columns considering semi-rigid connections. Akbaş and Kocatürk (2013) and Kocatürk and Akbaş (2013) investigated the post-buckling behavior of temperature-dependent and position-dependent functionally graded beam structures by using the finite element method. Li and Batra (2013) proposed analytical relations between the critical buckling load of an FGM Timoshenko beam and that of the corresponding homogeneous Euler–Bernoulli beam subjected to axial compressive load. Eltaher et al. (2013) presented the size-dependent static-buckling behavior of functionally graded (FG) nano-beams on the basis of the nonlocal continuum model. Reddy (2000) presented a theoretical formulation and finite element models based

on the third-order shear deformation of the FG plates theory to investigate the buckling behavior of these structures. Bouazza et al. (2017) used a new hyperbolic shear deformation theory to study the mechanical buckling analysis of functionally graded plates, where the presented theory has only four unknown functions as against five in case of Mindlin-Reissner theory. Meksi et al. (2018) proposed a numerical procedure for the buckling analysis of FGM plates having parabolic-concave thickness variation. Khalid (2018) studied the buckling characteristics of both nonlinear symmetric power and sigmoid FGM beams using the finite element method.

According to the literature, there is no antecedent study on buckling analysis of FGM beams with arbitrary boundary conditions, including various effects of power-law index and transverse shear. In this paper, critical buckling loads are examined and presented with details based on Euler–Bernoulli and Timoshenko beam theories, by using finite element method. A brief historical overview of these theories could be found in Han et al. (1999). The stiffness and the geometrical stiffness matrix of FGM beams are given in detail as they have not been presented before. The variation of material properties is along the beam thickness and is assumed to trail a power-law of the volume fraction of the constituents, usually ceramic and metal. Finite element numerical results are presented in both tabular and graphical forms to figure out the effects of power-law index, slenderness ratio and boundary conditions on the buckling behavior of FGM beams.

To our best knowledge, there is no reported work on the importance of including the transverse shear to predict critical loads for FGM beams in the literature. It is believed that the presented results will provide a reference with which other researchers can compare their results.

FGM BEAM MATERIAL PROPERTIES

FGM beam material properties vary continuously and non-uniformly in the z direction as derived by:

$$V_c = \left(\frac{z}{h} + \frac{1}{2}\right)^p \tag{1-a}$$

$$V_m = 1 - V_c \tag{1-b}$$

where p is the power-law index, the non-negative parameter which dictates the variation of material properties through the thickness of the beam. For $p = 0$, the volume fraction of ceramic becomes one and a homogeneous beam consisting only of ceramic is obtained. When the value of p is increased, the content of metal in FGM increases.

It is assumed that material properties of the beam, such as the modulus of elasticity E_{eff}, Poisson's ratio ν_{eff} and shear modulus G_{eff}, vary continuously through the beam thickness according to power-law form which can be described by:

$$MP_{eff} = MP_m V_m(z) + MP_c V_c(z) \tag{2}$$

where MP_m and MP_c stand for material properties of metal and ceramic, respectively.

FINITE ELEMENT FORMULATION

Euler-Bernoulli Beam Theory (EBT)

Using Euler-Bernoulli hypothesis, the axial and vertical displacements of any point of an FGM beam section are expressed as:

$$u(x,z) = u_0(x) - z\frac{\partial w_0}{\partial x} \tag{3-a}$$

$$w(x,z) = w_0(x) \tag{3-b}$$

where $u_0(x)$ and $w_0(x)$ are the axial and transverse displacements in the reference plane, in the x and z directions, respectively. Eqs. (3-a) and (3-b) can be rewritten in matrix form as:

$$\begin{Bmatrix} u \\ w \end{Bmatrix} = \begin{bmatrix} 1 & 0 & -z \\ 0 & 1 & 0 \end{bmatrix} \begin{Bmatrix} u_0 \\ w_0 \\ \dfrac{\partial w_0}{\partial x} \end{Bmatrix} \tag{4}$$

By assuming small deformations, the displacement-strain relation can be represented as:

$$\begin{aligned} &\varepsilon_{xx} = \frac{\partial u}{\partial x} = \varepsilon_{xx}^0 + z\kappa_{xx} \\ &\varepsilon_{xx}^0 = \frac{\partial u_0}{\partial x},\ \kappa_{xx} = -\frac{\partial^2 w_0}{\partial x^2} \end{aligned} \tag{5-a}$$

or

$$\varepsilon_{xx} = \begin{bmatrix} 1 & -z \end{bmatrix} \begin{Bmatrix} \dfrac{\partial u_0}{\partial x} \\ \dfrac{\partial^2 w_0}{\partial x^2} \end{Bmatrix} \tag{5-b}$$

ε_{xx}^0 and κ_{xx} are the extensional strain and the bending strain, respectively.

According to the Hooke's law, the normal stress is defined as:

$$\sigma_{xx} = E(z)\varepsilon_{xx} = E(z)\begin{bmatrix} 1 & -z \end{bmatrix} \begin{Bmatrix} \dfrac{\partial u_0}{\partial x} \\ \dfrac{\partial^2 w_0}{\partial x^2} \end{Bmatrix} \tag{6}$$

where *E(z)* is the variation of the Young's modulus through the thickness direction (z).

Based on the principle of the minimum potential energy which states that, if a body is in equilibrium, the total of the virtual strain energy done by internal forces and the virtual potential of external loadings is zero.

$$\delta\pi = \delta(U_I + W_E) = 0 \tag{7}$$

δU_I and δW_E are given as:

$$\delta U_I = \int_V \sigma_{xx}\delta\varepsilon_{xx} dV = \int_0^L \left(N\delta\varepsilon_{xx}^0 + M\delta\kappa_{xx}^0\right) dx \tag{8}$$

$$\delta W_E = \int_0^L \left(\bar{N}\frac{\partial w_0}{\partial x}\frac{\partial \delta w_0}{\partial x} + q\delta w_0 + f\delta u_0\right) dx \tag{9}$$

N is the normal force and M is the bending moment across the FGM beam section, defined as:

$$N = \int_A \sigma_{xx} dA = \hat{D}_a\,\varepsilon_{xx}^0 + \hat{D}_{ab}\,\kappa_x \tag{10}$$

$$M = \int_A z\,\sigma_{xx} dA = \hat{D}_{ab}\,\varepsilon_{xx}^0 + \hat{D}_b\,\kappa_x \tag{11}$$

$\hat{D}_a$ is the axial stiffness, $\hat{D}_b$ is the bending stiffness and $\hat{D}_{ab}$ is the coupling axial-bending stiffness. These stiffness coefficients can be calculated by:

$$\begin{bmatrix} \hat{D}_a & \hat{D}_b & \hat{D}_{ab} \end{bmatrix} = b\int_{-h/2}^{+h/2} E(z)\begin{bmatrix} 1 & z^2 & z \end{bmatrix} dz \tag{12}$$

$\bar{N}$ is the applied axial compressive load, f and q are the distributed forces in x and z directions, respectively.

By substituting Eqs. (8) and (9) into Eq.(7), integrating by parts and equating to zero the coefficients δu_0 and δw_0, the following expressions are obtained.

$$\frac{\partial N}{\partial x} + f = 0 \tag{13}$$

$$\frac{\partial^2 M}{\partial x^2} + q - \frac{\partial}{\partial x}\left(\bar{N}\frac{\partial w_0}{\partial x}\right) = 0 \tag{14}$$

The variational statement of FGM Euler-Bernoulli beam can be obtained by substituting Eqs. (10) and (11) into Eqs. (13) and (14) and therefore into eq. (7):

$$\int_0^L \left[\begin{aligned} &\left\{-b\int_{-h/2}^{+h/2} E(z)dz\right\}\frac{\partial u_0}{\partial x}\frac{\partial \delta u_0}{\partial x} + \left\{b\int_{-h/2}^{+h/2} zE(z)dz\right\}\frac{\partial^2 w_0}{\partial x^2}\frac{\partial \delta u_0}{\partial x} + \\ &\left\{b\int_{-h/2}^{+h/2} zE(z)dz\right\}\frac{\partial u_0}{\partial x}\frac{\partial^2 \delta w_0}{\partial x^2} - \left\{b\int_{-h/2}^{+h/2} z^2E(z)dz\right\}\frac{\partial^2 w_0}{\partial x^2}\frac{\partial^2 \delta w_0}{\partial x^2} \\ &+ f\delta u_0 + q\delta w_0 + \bar{N}\frac{\partial w_0}{\partial x}\frac{\partial \delta w_0}{\partial x} \end{aligned}\right] dx = 0 \tag{15}$$

Finite Element Modeling

The displacement components can be written by using shape functions and nodal displacements. They can be expressed as a result of axial and transverse components as shown below.

• ***Axial components***

$$U(x)=\left[N(x)\right]_u\left\{q\{t\}\right\}_u \tag{16}$$

• ***Transverse components***

$$W(x)=\left[N(x)\right]_w\left\{q\{t\}\right\}_w \tag{17}$$

$\left[N(x)\right]$ and $q\{t\}$ represent the shape functions and nodal displacements, respectively.

By substituting Eqs. (16) and (17) into Eq. (15) and integrating it over domain, the finite element system of equations can be written in a compact form as follows:

$$\left[K\right]\{q\}=\lambda\left[K_G\right]\{q\} \tag{18}$$

where λ is the buckling load, $\left[K\right]$ and $\left[K_G\right]$ represent the global stiffness matrix and the global geometric stiffness matrix of FGM beam, as defined in Appendix A.

Timoshenko Beam Theory (TBT)

Based on Timoshenko beam theory, the axial and vertical displacements of any point of the beam section are expressed as:

$$u(x,z)=u_0(x)-z\theta_z(x) \tag{19}$$

$$w(x,z)=w_0(x) \tag{20}$$

where u_0 and w_0 are the axial and the transverse displacements of any point on the mid-plane, respectively and θ_z is the bending rotation. Eqs. (19) and (20) can be rewritten as:

$$\begin{Bmatrix}u\\w\end{Bmatrix}=\begin{bmatrix}1&0&-z\\0&1&0\end{bmatrix}\begin{Bmatrix}u_0\\w_0\\\theta_z\end{Bmatrix} \tag{21}$$

The nonzero strains can be represented by:

$$\varepsilon_{xx}=\frac{\partial u}{\partial x}=\frac{\partial u_0}{\partial x}-z\frac{\partial \theta_z}{\partial x},\ \gamma_{xz}=\frac{\partial u}{\partial z}+\frac{\partial w}{\partial x}=-\theta_z+\frac{\partial w_0}{\partial x} \tag{22-a}$$

or

$$\varepsilon=\begin{Bmatrix}\varepsilon_{xx}\\\gamma_{xz}\end{Bmatrix}=\begin{bmatrix}1&-z&0\\0&0&1\end{bmatrix}\begin{bmatrix}\frac{\partial u_0}{\partial x}&\frac{\partial \theta_z}{\partial x}&\frac{\partial w_0}{\partial x}-\theta_z\end{bmatrix}^T \tag{22-b}$$

The constitutive relation for FGM is assumed to be of the form

$$\sigma_{xx}=E(z)\varepsilon_{xx}=E(z)\left(\frac{\partial u_0}{\partial x}-z\frac{\partial \theta_z}{\partial x}\right) \tag{23}$$

$$\tau_{xz}=G(z)\gamma_{xz}=G(z)\left(-\theta_z+\frac{\partial w_0}{\partial x}\right) \tag{24}$$

It can be expressed in matrix form as follows:

$$\sigma=\begin{Bmatrix}\sigma_{xx}\\\tau_{xz}\end{Bmatrix}=\begin{bmatrix}E(z)&0\\0&G(z)\end{bmatrix}\begin{Bmatrix}\varepsilon_{xx}\\\gamma_{xz}\end{Bmatrix} \tag{25-a}$$

$$\sigma=\begin{Bmatrix}\sigma_{xx}\\\tau_{xz}\end{Bmatrix}=\begin{bmatrix}E(z)&0\\0&G(z)\end{bmatrix}\begin{bmatrix}1&-z&0\\0&0&1\end{bmatrix}\begin{bmatrix}\frac{\partial u_0}{\partial x}&\frac{\partial \theta_z}{\partial x}&\frac{\partial w_0}{\partial x}-\theta_z\end{bmatrix}^T \tag{25-b}$$

In accordance with the same procedure that was applied for Euler-Bernoulli beam theory, the normal force, the shear force and the bending moment of the Timoshenko FGM beam can be obtained as follows:

$$N=\int_A\sigma_{xx}dA=\hat{D}_a\,\varepsilon_{xx}^0+\hat{D}_{ab}\,\kappa_x \tag{26}$$

$$Q=\int_A\kappa_s\sigma_{xz}dA=\kappa_s\hat{D}_s\left(\frac{\partial w}{\partial x}-\theta_z\right) \tag{27}$$

$$M=\int_A z\,\sigma_{xx}dA=\hat{D}_{ab}\,\varepsilon_{xx}^0+\hat{D}_b\,\kappa_x \tag{28}$$

where $\left[\hat{D}_s\right]=b\int_{-h/2}^{+h/2}G(z)dz$

For anisotropic beam, the term containing $\widehat{D}_{ab}$ is equal zero, because there is no membrane-bending coupling.

The stiffness matrix and the geometric stiffness matrix of Timoshenko beam theory are given in Appendix B.

NUMERICAL RESULTS AND DISCUSSION

This part is divided into two subsections; the first subsection is devoted mainly to verify the present model with those previously published for homogenous ceramic beam. The second subsection is reserved for FGM beams. Therefore, FORTRAN codes are developed. An FGM beam with different lengths is considered, the material properties of ceramic are $E_c = 380GPa$, $\nu_c = 0,23$ and those of metal are $E_m = 70GPa$, $\nu_m = 0,23$.

The non-dimensional critical buckling load is computed by the following formula:

$$P = \frac{\lambda L^2}{E_M I} \tag{29}$$

Model Validation

For validation, a comparison of dimensionless critical loads for homogenous ceramic beam using Euler-Bernoulli beam theory is performed and the results are shown in Table 1. It can be observed that the predicted results given by the present method are in good agreement with those given by Li and Batra (2013) for all boundary conditions and for all length to thickness ratios.

Table 1. Comparison of dimensionless critical loads for different boundary conditions (EBT theory)

L/h	C-C		C-S		S-S		C-F	
	Present study	**Li and Batra (2013)**	**Present study**	**Li and Batra (2013)**	**Present study**	**Li and Batra (2013)**	**Present study**	**Li and Batra (2013)**
5	214.35	214.31	109.61	109.61	53.578	53.578	13.394	13.394
10	214.35	214.31	109.61	109.61	53.578	53.578	13.394	13.394

Parametric Results

After validation of the isotropic beam, the finite element method is extended to study the FGM beam buckling behavior for various slenderness ratios, power-law indices and end boundary conditions.

Simply Supported Beam (S-S)

The effects of geometrical parameters and material distribution profile on the non-dimensional critical loads of simply supported beam, using two beam formulations, are exhibited in Table 2 and Fig. 1. It is interesting to note that all the values of critical loads decrease with an increase of the power-law index. Furthermore, the difference between the values predicted by EBT and TBT theories get more pronounced at small values of length to thickness ratio, which confirms the importance of using the TBT theory for non-slender beam, as the slenderness ratio has no significant effect on critical loads for EBT theory. Similar results have been shown using plots in Fig. 1, for a constant power-law index, where critical loads do not match for lower values of length to thickness ratio, which emphasizes the effect of transverse shear that increases the flexibility of thick beams and therefore reduces critical loads. The two curves coincide after L/h =20.

Table 2. Effects of (L/h) and power-law index (p) on non-dimensional critical loads for (S-S) beam

L/h	Theories	p=0	p=1	p=2	p=5
5	EBT	53.5786	26.7412	20.8808	17.6547
	TBT	48.8680	24.7319	19.2921	16.0615
	% Error	9.6394	8.1242	8.2346	9.9200
10	EBT	53.5786	26.7412	20.8808	17.6547
	TBT	52.3184	26.2091	20.4598	17.2277
	% Error	2.4086	2.0301	2.0577	2.4786
20	EBT	53.5786	26.7412	20.8808	17.6547
	TBT	53.2579	26.6062	20.7739	17.5460
	% Error	0.6021	0.5075	0.5144	0.6196
50	EBT	53.5786	26.7412	20.8808	17.6547
	TBT	53.5270	26.7195	20.8636	17.6373
	% Error	0.0963	0.0812	0.0823	0.0991
100	EBT	53.5786	26.7412	20.8808	17.6547
	TBT	53.5657	26.7358	20.8765	17.6504
	% Error	0.0241	0.0203	0.0206	0.0248

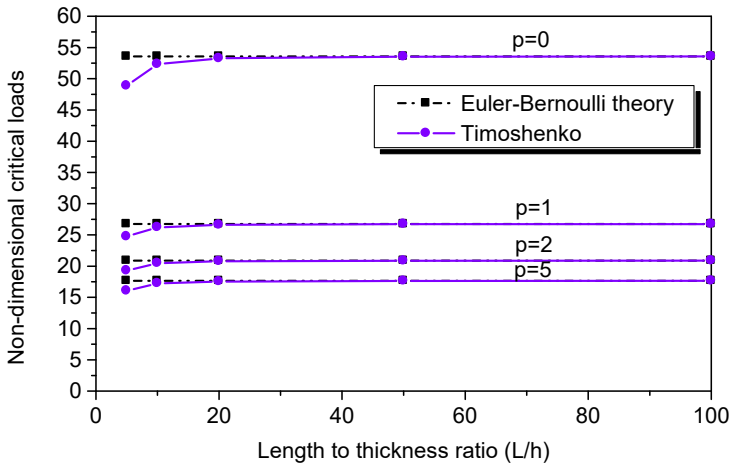

Figure (1): Variation of non-dimensional critical loads with respect to p and L/h (S-S)

Clamped-Clamped Beam (C-C)

Table 3 and Fig. 2 illustrate the effects of slenderness ratio and power-law index on buckling loads for clamped beam. As mentioned earlier, the values obtained with Timoshenko beam theory converged to those obtained by Euler-Bernoulli theory after L/h=50

and the two curves got closer after L/h=50. It is important to note that for the same L/h ratio, the maximum difference is observed for C-C beam as compared with the other end conditions.

Table 3. Effects of (L/h) and power-law index (p) on non-dimensional critical loads for (C-C) beam

L/h	Theories	p=0	p=1	p=2	p=5
5	EBT	214.3569	107.3951	84.0216	70.9951
	TBT	155.3849	81.3155	63.3788	50.9819
	% Error	37.9522	32.0721	32.5704	39.2554
10	EBT	214.3569	107.3951	84.0216	70.9951
	TBT	195.8865	99.4648	77.7285	64.6875
	% Error	9.4291	7.9730	8.0962	9.7509
20	EBT	214.3569	107.3951	84.0216	70.9951
	TBT	209.4304	105.3001	82.3577	69.3092
	% Error	2.3523	1.9896	2.0203	2.4324
50	EBT	214.3569	107.3951	84.0216	70.9951
	TBT	213.5536	107.0545	83.7510	70.7201
	% Error	0.3761	0.3182	0.3231	0.3889
100	EBT	214.3569	107.3951	84.0216	70.9951
	TBT	214.1555	107.3098	83.9538	70.9261
	% Error	0.0940	0.0795	0.0808	0.0972

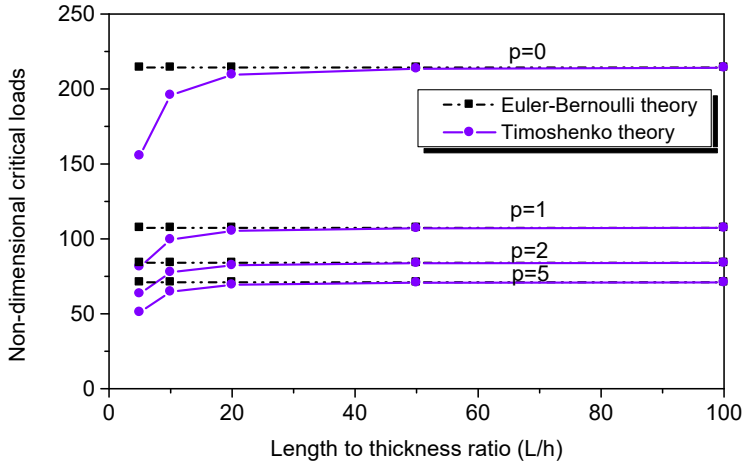

Figure (2): Variation of non-dimensional critical loads with respect to p and L/h (C-C)

Clamped-Simply Supported Beam (C-S)

The effects of slenderness ratio and power-low index on non-dimensional critical loads in case of clamped-simply supported beam are exhibited in Table 4 and Fig. 3. The response of this beam goes between the S-S and C-C counterparts.

Table 4. Effects of (L/h) and power-law index (p) on non-dimensional critical loads for (C-S) beam

L/h	Theories	p=0	p=1	p=2	p=5
5	EBT	109.6129	54.7961	42.8222	36.1966
	TBT	90.1716	46.3602	36.1495	29.6121
	% Error	21.5604	18.1964	18.4586	22.2356
10	EBT	109.6129	54.7961	42.8222	36.1966
	TBT	104.0160	52.4153	40.9361	34.2936
	% Error	5.3809	4.5421	4.6075	5.5491
20	EBT	109.6129	54.7961	42.8222	36.1966
	TBT	108.1588	54.1812	42.3348	35.7016
	% Error	1.3445	1.1350	1.1513	1.3865
50	EBT	109.6129	54.7961	42.8222	36.1966
	TBT	109.3777	54.6968	42.7435	36.1165
	% Error	0.2151	0.1816	0.1842	0.2218
100	EBT	109.6129	54.7961	42.8222	36.1966
	TBT	109.5540	54.7712	42.8025	36.1765
	% Error	0.0538	0.0454	0.0460	0.0555

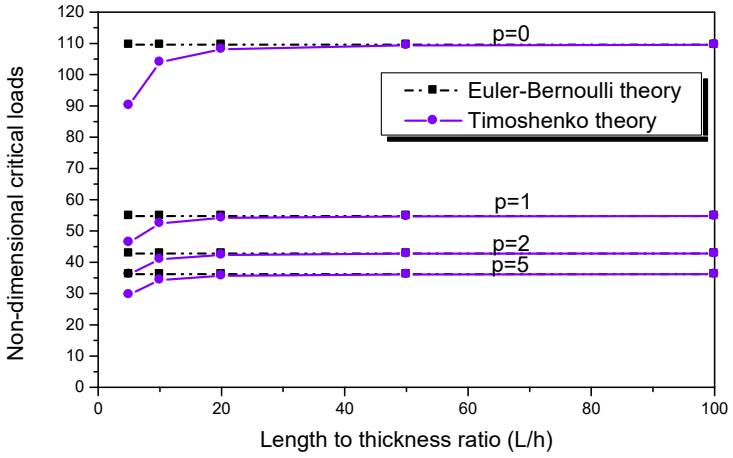

Figure (3): Variation of non-dimensional critical loads with respect to p and L/h (C-S)

Clamped-Free Beam (C-F)

Table 5 and Fig. 4 reveal the effects of slenderness ratio and power-law index on buckling loads for clamped-free beam. As can be observed, the shear effects are less predominant after L/h=50. As the values of length to thickness ratio approach 100, the difference

among the two theories fades and becomes negligible as shown in Fig. 4.

Fig. 5 highlight, the effects of power-law index and length-to-thickness ratio on non-dimensional critical buckling loads for C-C FGM beams. It is seen that when the power-law index increases, critical buckling loads show a downward trend. Maximum critical buckling load values are obtained for full ceramic beams (p=0). When the value of p is increased, the content of metal in FGM increases. This is due to the fact that an increase in the value of power-law index results in a decrease in the value of elasticity modulus. In other words, the beam becomes flexible as the power-law index increases, thus decreasing critical buckling load values.

Table 5. Effects of (L/h) and power-law index (p) on non-dimensional critical loads for (C-F) beam

L/h	Theories	p=0	p=1	p=2	p=5
5	EBT	13.3945	6.6787	5.2125	4.4079
	TBT	13.0776	6.5452	5.1069	4.3008
	% Error	2.4231	2.0404	2.0671	2.4903
10	EBT	13.3945	6.6787	5.2125	4.4079
	TBT	13.3138	6.6448	5.1857	4.3806
	% Error	0.6057	0.5101	0.5168	0.6226
20	EBT	13.3945	6.6787	5.2125	4.4079
	TBT	13.3742	6.6702	5.2058	4.4011
	% Error	0.1514	0.1275	0.1292	0.1556
50	EBT	13.3945	6.6787	5.2125	4.4079
	TBT	13.3912	6.6774	5.2114	4.4068
	% Error	0.0242	0.0204	0.0207	0.0249
100	EBT	13.3945	6.6787	5.2125	4.4079
	TBT	13.3937	6.6784	5.2122	4.4076
	% Error	0.0061	0.0051	0.0052	0.0062

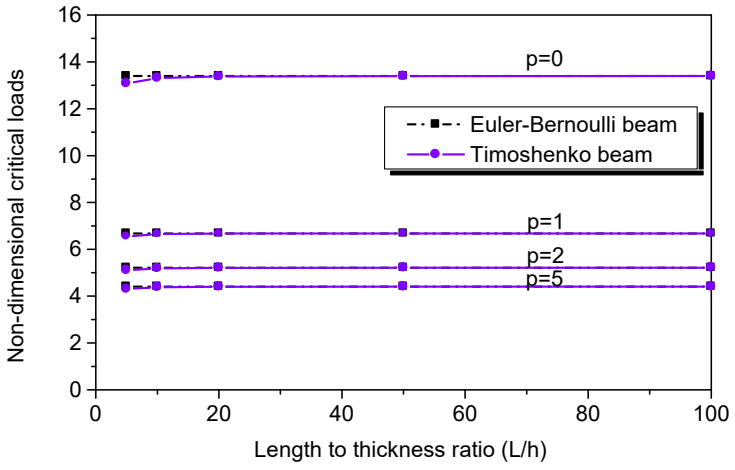

Figure (4): Variation of non-dimensional critical loads with respect to p and L/h (C-F)

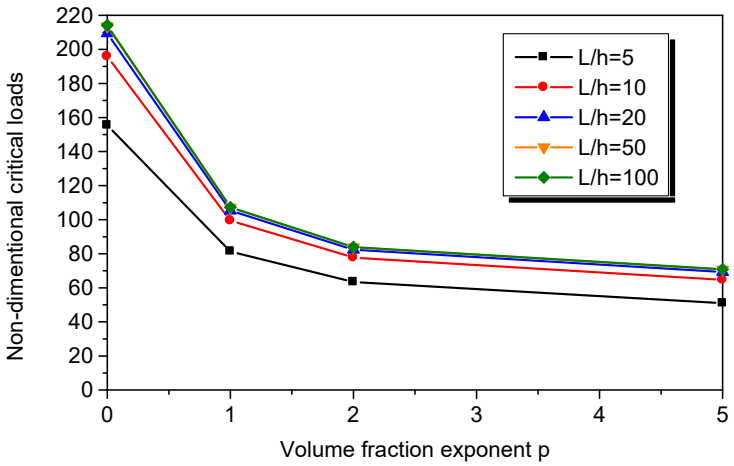

Figure (5): Variation of non-dimensional critical buckling loads with respect to power-law index and length-to-thickness ratio for clamped-clamped FGM beams (TBT)

CONCLUSIONS

In this research, a complete investigation on the significance of transverse shear for the buckling analysis of beams made of FGM is performed. To this end, two engineering beam theories are presented, one neglecting transverse shear (Euler-Bernoulli theory) and the other considering transverse shear (Timoshenko theory). It is shown through numerical results that by introducing transverse shear, the flexibility of the short beam increases and therefore reduces critical loads. It can be also deduced that the transverse shear is more prominent with C-C end conditions compared to S-S, C-S and C-F counterparts. By the way, the values of the critical loads with C-C beam are higher than those for the other boundary conditions. Accordingly, FGM beams with C-C boundary conditions are more affected by slenderness ratio compared to the other boundary conditions. It is also interesting to note that the accuracy of Timoshenko beam theory is higher than that of the Euler-Bernoulli beam theory. Euler-Bernoulli model tends to slightly overestimate critical loads for non-slender beam. The results also show that, with raising the material gradient index, non-dimensional critical loads decreases.

It is inferred that, in the design of structures with non-slender ratio, transverse shear should be considered to better predict the critical loads in FGM beam type structures.

APPENDIX A

Euler-Bernoulli Beam Theory

The global stiffness matrix for Euler-Bernoulli beam is:

$$[K]=\begin{bmatrix} \frac{\hat{D}_a}{L} & 0 & \frac{-\hat{D}_{ab}}{L} & \frac{-\hat{D}_a}{L} & 0 & \frac{\hat{D}_{ab}}{L} \\ 0 & \frac{12\hat{D}_b}{L^3} & \frac{6\hat{D}_b}{L^2} & 0 & \frac{-12\hat{D}_b}{L^3} & \frac{6\hat{D}_b}{L^2} \\ & & \frac{4\hat{D}_b}{L^2} & \frac{\hat{D}_{ab}}{L} & \frac{-6\hat{D}_b}{L^2} & \frac{2\hat{D}_b}{L} \\ & & & \frac{\hat{D}_a}{L} & 0 & \frac{-\hat{D}_{ab}}{L} \\ & & & & \frac{12\hat{D}_b}{L^3} & \frac{-6\hat{D}_b}{L^2} \\ & & & & & \frac{4\hat{D}_b}{L} \end{bmatrix}$$

The global geometric stiffness matrix for Euler-Bernoulli beam is:

$$[K_G]=\frac{\overline{N}}{L}\begin{bmatrix} 0 & 0 & 0 & 0 & 0 & 0 \\ & \frac{6}{5} & \frac{L}{10} & 0 & \frac{-6}{5} & \frac{L}{10} \\ & & \frac{2L^2}{15} & 0 & \frac{-L}{10} & \frac{-L^2}{30} \\ & & & 0 & 0 & 0 \\ & & & & \frac{6}{5} & \frac{-L}{10} \\ & & & & & \frac{2L^2}{15} \end{bmatrix}$$

APPENDIX B

Timoshenko Beam Theory

The global stiffness matrix for Timoshenko beam is:

$$[K]=\begin{bmatrix} \frac{\hat{D}_a}{L} & 0 & \frac{-\hat{D}_{ab}}{L} & \frac{-\hat{D}_a}{L} & 0 & \frac{\hat{D}_{ab}}{L} \\ 0 & \frac{12\hat{D}_b}{L^3(1+\phi_z)} & \frac{6\hat{D}_b}{L^2(1+\phi_z)} & 0 & \frac{-12\hat{D}_b}{L^3(1+\phi_z)} & \frac{6\hat{D}_b}{L^2(1+\phi_z)} \\ & & \frac{\hat{D}_b(4+\phi_z)}{L(1+\phi_z)} & \frac{\hat{D}_{ab}}{L} & \frac{-6\hat{D}_b}{L^2(1+\phi_z)} & \frac{\hat{D}_b(2-\phi_z)}{L(1+\phi_z)} \\ & & & \frac{\hat{D}_a}{L} & 0 & \frac{-\hat{D}_{ab}}{L} \\ & & & & \frac{12\hat{D}_b}{L^3(1+\phi_z)} & \frac{-6\hat{D}_b}{L^2(1+\phi_z)} \\ & & & & & \frac{\hat{D}_b(4+\phi_z)}{L(1+\phi_z)} \end{bmatrix}$$

The global geometric stiffness matrix for Timoshenko beam is:

$$[K_G]=\frac{\overline{N}}{(1+\phi_y)^2}\begin{bmatrix} 0 & 0 & 0 & 0 & 0 & 0 \\ & p_1 & p_2 & 0 & p_3 & p_4 \\ & & p_5 & 0 & p_6 & p_7 \\ & & & 0 & 0 & 0 \\ & & & & p_8 & p_9 \\ & & & & & p_{10} \end{bmatrix}$$

$$p_1 = \frac{6}{5L} + \frac{2\phi_z}{L} + \frac{\phi_z^2}{L} \qquad p_6 = \frac{-1}{10}$$

$$p_2 = \frac{1}{10} \qquad p_7 = \frac{-L}{30} - \frac{\phi_z L}{6} - \frac{\phi_z{}^2 L}{12}$$

$$p_3 = \frac{-6}{5L} - \frac{2\phi_z}{L} - \frac{\phi_z^2}{L} \qquad p_8 = \frac{6}{5L} + \frac{2\phi_z}{L} + \frac{\phi_z^2}{L}$$

$$p_4 = \frac{1}{10} \qquad p_9 = \frac{-1}{10}$$

$$P_5 = \frac{2L}{15} + \frac{\phi_z L}{6} + \frac{\phi_z^2 L}{12} \qquad p_{10} = \frac{2L}{15} + \frac{\phi_z L}{6} + \frac{\phi_z^2 L}{12}$$

REFERENCES

Akbaş, Ş. D. (2015). "Post-buckling analysis of axially functionally graded three-dimensional beams". International Journal of Applied Mechanics, 7 (3), 1550047.

Akbaş Ş. D., and Kocatürk T. (2013). "Post-buckling analysis of functionally graded three-dimensional beams under the influence of temperature". Journal of Thermal Stresses, 36 (12), 1233-1254.

Bouazza, M., Amara, K., and Benseddiq, N. (2017). "Mechanical buckling analysis of functionally graded plates using a new refined theory". Jordan Journal of Civil Engineering, 11 (1), 64-79.

Eltaher, M.A., Emam, S.A., and Mahmoud, F.F. (2013). "Static and stability analysis of nonlocal functionally graded nanobeams". Composite Structures, 96, 82-88.

Han, S.M., Benaroya, H. and Wei, T. (1999). "Dynamics of transversely vibrating beams using four engineering theories". Journal of Sound and Vibration, 225 (5), 935-988.

Khalid Almitani, H. (2018). "Buckling behaviors of symmetric and antisymmetric functionally graded beams". Journal of Applied and Computational Mechanics, 4 (2), 115-124.

Kocaturk, T., and Akbas S.D. (2013). "Thermal post-buckling analysis of functionally graded beams with temperature-dependent physical properties". Steel and Composite Structures, 15 (5), 481-505.

Li, S. R., and Batra R. C. (2013). "Relations between buckling loads of functionally graded Timoshenko and homogeneous Euler–Bernoulli beams". Composite Structures, 95, 5-9.

Meksi, A., Belakhdar, K., Bouguenina, O., Tounsi, A., and Bedia El-Abbes, Adda. (2018). "Effect of parabolic-concave thickness variation on the mechanical buckling resistance of simply supported FGM plates". Jordan Journal of Civil Engineering, 12 (2), 216-227.

Reddy, J. N. (2000). "Analysis of functionally graded plates". International Journal for Numerical Methods in Engineering, 47 (1-3), 663-684.

Rezaiee-Pajand, M., and Masoodi, A.R. (2016). "Exact natural frequencies and buckling load of functionally graded material tapered beam-columns considering semi-rigid connections". Journal of Vibration and Control, 24 (9), 1787-1808.